Journal of Inorganic and General Chemistry
ZAAC
Zeitschrift für anorganische und allgemeine Chemie
www.zaac.wiley-vch.de
RESEARCH ARTICLE

Check for updates

DOI: 10.1002/zaac.202500044

Hf_6Al_7 and $Hf_{4.44(1)}Nb_{1.56(1)}Al_7$—the First Fully Ordered Main Group Metal Containing W_6Fe_7 Type Compound and its Ternary Coloring Variant

Elias C. J. Gießelmann, Lena Ruck, Stefan Engel, Bernd Morgenstern, Lars Schumacher, Guido Kickelbick, and Oliver Janka*

Dedicated to Professor Gordon Miller on the Occasion of his 65th Birthday

Attempts to synthesize Hf_4NbAl_7 led to the discovery of nominal $Hf_4Nb_2Al_7$ instead of the envisioned product. It was identified based on powder diffraction data. The compound can be described as a substitutional/coloring variant of the rhombohedral W_6Fe_7 type structure (space group $R\bar{3}m$). The formation of the ternary compound motivates the synthesis of the binary compound Hf_6Al_7. Different synthetic strategies lead to its discovery. The crystal structures of the binary as well as its ternary coloring variant are refined from single-crystal X-ray diffraction data showing both the same obverse–reverse twinning. For the Nb-containing phase, a composition of $Hf_{4.44(1)}Nb_{1.56(1)}Al_7$ is refined, in agreement with the powder X-ray data. Solid-state ^{27}Al NMR investigations indicate the formation of a crystalline compound; however, only one distinct signal can be observed in contrast to the two crystallographic Al positions. Magnetic susceptibility measurements confirm the expected Pauli-paramagnetic character. Quantum-chemical calculations alongside analyses of the chemical bonding with the LOBSTER program package show that a strong Hf–Hf interaction is present, which transforms into an even stronger Nb–Nb interaction in nominal $Hf_4Nb_2Al_7$. For the latter, three substitutional variants are calculated, clearly indicating the experimentally observed one as the most stable.

1. Introduction

Intermetallic aluminum compounds of the general composition $M_xT_yAl_z$ containing two early transition metals (e.g., M = group 4; T = group 5) are rather scarcely investigated and structurally characterized. The Pearson database[1] lists less than 100 entries when searching for M = Ti, Zr and Hf and T = V, Nb alongside Al. The majority of these entries are solid solutions in various structure types. Besides a mixture of all three elements on one crystallographic position, e.g., in the Mg ($P6_3/mmm$)[2] or W ($Im\bar{3}m$) type structure,[3] a significant number of entries are reported to adopt the tetragonal CuAu ($P4/mmm$)[4] or $TiAl_3$ ($I4/mmm$)[5] or the rhombohedral W_6Fe_7 ($R\bar{3}m$) type structures.[6] As for the fully ordered compounds, only $Ti_4Nb_3Al_9$ ($P4/mmm$, own type)[7] and the recently reported Hf_4VAl_7 ($P\bar{3}m1$, own type)[8] are known. The latter is a new superstructure and ternary ordering variant of $HfAl_2$,[9] which adopts the hexagonal Laves phase ($P6_3/mmc$, $MgZn_2$ type structure[10]) and was found during phase analytical investigations in the ternary system Hf–V–Al.[8] When changing to the lighter homologue of Hf, Zr, no distinct superstructures of Laves phases or any ternary ordering variant could be observed.[11] Recent review articles summarize the concept of coloring and ordering variants of Laves phases.[12,13]

Upon attempts to synthesize Hf_4NbAl_7, in analogy to Hf_4VAl_7,[8] a $MgZn_2$ type Laves phase, $Hf(Nb_{1-x}Al_x)_2$ was observed alongside a compound crystallizing in the W_6Fe_7 type structure. The latter had been reported by Fedorova as $Hf_{3.6}Nb_{2.3}Al_{7.1}$ with mixing of Hf, Nb, and Al on the three crystallographic W positions of the prototype.[14] In the rhombohedral W_6Fe_7 type structure ($R\bar{3}m$),[6] three W positions ($3 \times 6c$) and two Fe ($3b$ and $18h$) are present. The compound can be classified as a so-called Frank–Kasper phase. Frank–Kasper phases can be viewed as topologically closed packed structures with high coordination numbers (CNs) of CN = 12, 14, 15, and 16. All coordination polyhedra exhibit solely triangular faces and are strongly interpenetrating.[15,16] Examples for these Frank–Kasper phases are the A15 phases (Cr_3Si type),[17,18] the Laves phases ($MgCu_2$, $MgZn_2$ and $MgNi_2$ types),[12,17–19] and the aforementioned μ phases with W_6Fe_7 being one representative. For this specific structure type, the majority of compounds known are formed with an early transition metal (Nb, Ta, Mo, or W) together with a 3*d* transition metal (Fe, Co, Ni, and Zn). The only main group element that was reported in this structure type is Si, however, with a composition of $\approx Mn_{11}Si_2$ showing severe Mn/Si disorder.[1]

E. C. J. Gießelmann, L. Ruck, S. Engel, B. Morgenstern, G. Kickelbick, O. Janka
Solid State Inorganic Chemistry, Saarland University, Campus C4 1, 66123 Saarbrücken, Germany
E-mail: oliver.janka@uni-saarland.de
L. Schumacher
Institut für Anorganische und Analytische Chemie, Universität Münster, Corrensstrasse 28/30, 48149 Münster, Germany

Supporting information for this article is available on the WWW under https://doi.org/10.1002/zaac.202500044

© 2025 The Author(s). Zeitschrift für anorganische und allgemeine Chemie published by Wiley-VCH GmbH. This is an open access article under the terms of the Creative Commons Attribution License, which permits use, distribution and reproduction in any medium, provided the original work is properly cited.

15213749, 2025, 11, Downloaded from https://onlinelibrary.wiley.com/doi/10.1002/zaac.202500044 by Universitatsbibliothek Der, Wiley Online Library on [11/08/2025]. See the Terms and Conditions (https://onlinelibrary.wiley.com/terms-and-conditions) on Wiley Online Library for rules of use; OA articles are governed by the applicable Creative Commons License

In this contribution, we report on our successful syntheses of the new binary phase Hf_6Al_7 alongside its ternary coloring variant with a nominal composition close to $Hf_4Nb_2Al_7$ (both W_6Fe_7 type) and their spectroscopic characterization and the analysis of the peculiar chemical bonding.

2. Experimental Section

2.1. Synthesis

Initially, Hf_4NbAl_7 was targeted in analogy to the recently reported Hf_4VAl_7. The latter exhibited a new ternary ordering variant of the hexagonal Laves phase $MgZn_2$.[8] After phase analysis and identification of the formed products (vide infra), Hf_6Al_7 and nominal $Hf_4Nb_2Al_7$ were synthesized on-stoichiometry. All samples were prepared from the elements using hafnium and niobium pieces and aluminum turnings (all Onyxmet, Olsztyn, Poland) with stated purities above 99.5%. Samples were prepared on a 150 to 300 mg scale. For the reaction, the elements were arc-melted[20] in water-cooled copper crucible in an argon atmosphere of about 800 mbar with the different molar ratios given in Table S1 (Supporting Information). The argon gas was purified over titanium sponge (873 K), molecular sieves, and silica gel prior to the use. Subsequently, some of the arc-melted ingots were sealed in silica glass ampoules and heat-treated in muffle furnaces (Nabertherm 11/HR, Lilienthal/Bremen, Germany) with different temperature schemes for different lengths. A summary of the conducted syntheses alongside their analysis is given in Table S1 (Supporting Information). All melting beads are silver metallic; ground powders are grey. The samples were stable in air over weeks.

2.2. Powder and Single-Crystal X-Ray Diffraction

The pulverized samples of all discussed compounds were investigated by powder X-ray diffraction experiments at room temperature on a D8-A25-Advance diffractometer (Bruker-AXS, Karlsruhe, Germany) in Bragg-Brentano θ-θ-geometry (goniometer radius 280 mm) with non-monochromatic Cu $K_{\alpha1,2}$-radiation ($\lambda = 154.0596$ and 154.4425 pm). Diffraction patterns were recorded between 6 and 130° 2θ with a step size of 0.013° and a total scan time of 1 h. A 12 μm Ni foil working as K_β filter and a variable divergence slit were mounted at the primary beam side. On the secondary beam side, a LYNXEYE detector with 192 channels was used. The recorded data was evaluated using the Bruker TOPAS 5.0 software[21] employing the fundamental parameter approach and the Rietveld method.[22,23] Details regarding the refined sample compositions are listed in **Table 1**, the lattice parameters and refined compound compositions of the single-phase samples according to powder X-ray diffraction data are listed in **Table 2**. Additional powder X-ray patterns are shown in the electronic Supporting Information in Figure S1–S3.

From the annealed crushed samples, single crystals of Hf_6Al_7 and nominal $Hf_4Nb_2Al_7$ were isolated and investigated at room temperature on a Synergy-S diffractometer (Rigaku, Neu-Isenburg, Germany), operating with monochromatic Mo $K_{\alpha1}$ ($\lambda = 0.71073$ Å) radiation. Multiscan absorption corrections and scaling using the Crysalis program package[24] were applied to the data sets. The crystal structures were solved by direct methods using SHELXT[25] and refined by full matrix least squares calculations on F^2 (SHELXL2018[26]), part of the SHELX program package,[27] in the graphical user interface ShelXle.[28] Details on the structure refinement and atomic coordinates as well as interatomic distances are compiled in **Table** 2 and **3** and S2 (Supporting Information). Structural drawing were generated with Diamond 4[29] and edited with Adobe Illustrator CS6.

CSDs 2420799 and 2420800 contain the supplementary crystallographic data for this paper. The data can be obtained free of charge from The Cambridge Crystallographic Data Centre via www.ccdc.cam.ac.uk/structures.

2.3. Energy-Dispersive X-Ray Spectroscopy (EDX)

The powdered samples of Hf_6Al_7 and nominal $Hf_4Nb_2Al_7$ were semiquantitatively analyzed on a JEOL 7000F (JEOL, Freising, Germany) scanning electron microscope equipped with an EDAX Genesis 2000 EDX detector (EDAX, Unterschleissheim, Germany). The powdered samples were sprinkled on conductive carbon tape and one area scans as well as three independent data points were measured. The results of the SEM/EDX investigations are listed in **Table 4**.

Table 1. Lattice parameters and atomic positions, refined from powder X-ray diffraction, of Hf_6Al_7, $Hf_{4.30(1)}Nb_{1.70(1)}Al_7$, and literature data. Standard deviations, the *z* coordinates for Hf1, Hf2, Hf/Nb3, and Al2 as well as the occupational factor of the Hf/Nb3 position are given.

Compound	*a*/pm	*c*/pm	*V*/nm³	occ(Hf/Nb3)		References
Hf_6Al_7	530.10(1)	2912.18(6)	0.7087	1		*
$Hf_{3.6}Nb_{2.3}Al_{7.1}$	520	2850	0.6674	–		[14]
$Hf_{4.30(1)}Nb_{1.70(1)}Al_7$	525.27(1)	2864.63(5)	0.6845	0.15(1)/0.85(1)		*
	z(Hf1)	*z*(Hf2)	*z*(Hf/Nb3)	*x*(Al2)	*z*(Al2)	References
Hf_6Al_7	0.33430(6)	0.14938(7)	0.04534(5)	0.5112(2)	0.0900(2)	*
$Hf_{3.6}Nb_{2.3}Al_{7.1}$	no positional parameters determined					[14]
$Hf_{4.30(1)}Nb_{1.70(1)}Al_7$	0.33447(5)	0.14909(6)	0.04416(7)	0.5017(9)	0.0905(2)	*

*This work.

15213749, 2025, 11, Downloaded from https://onlinelibrary.wiley.com/doi/10.1002/zaac.202500044 by Universitatsbibliothek Der, Wiley Online Library on [11/08/2025]. See the Terms and Conditions (https://onlinelibrary.wiley.com/terms-and-conditions) on Wiley Online Library for rules of use; OA articles are governed by the applicable Creative Commons License

Table 2. Crystallographic data and structure refinement from single-crystal X-ray diffraction experiments for Hf_6Al_7 and $Hf_{4.44(1)}Nb_{1.56(1)}Al_7$ ($R\bar{3}m$, W_6Fe_7 type, $Z = 3$).

CSD number	2420800	2420799
Nominal composition	Hf_6Al_7	$Hf_4Nb_2Al_7$
Refined composition	Hf_6Al_7	$Hf_{4.44(1)}Nb_{1.56(1)}Al_7$
Lattice parameters a (pm)	530.49(1)	525.53(1)
c (pm)	2916.38(8)	2866.12(9)
V (nm^3)	0.71077	0.68552
Molar mass [g mol^{-1}]	1529.80	1125.95
Density calc. [g cm^{-3}]	8.83	8.18
Crystal size [μm]	40 × 10 × 10	50 × 10 × 10
Detector distance [mm]	31	31
Range in hkl	$h \pm 7$, $k \pm 7$, $l \pm 40$	$h \pm 8$, $k \pm 8$, $l \pm 47$
θ_{min}, θ_{max}, deg	4.193, 29.571	4.266, 36.262
Linear absorption coeff. [mm^{-1}]	66.0	52.7
No. of reflections	4948	6292
R_{int}/R_σ	0.0561/0.0154	0.0368/0.0140
No. of independent reflections	294	471
Reflections used [$I \geq 3\sigma(I)$]	289	464
$F(000)$, e	1569	1424
$R1/wR2$ for $I \geq 3\sigma(I)$	0.0156/0.0402	0.0181/0.0411
$R1/wR2$ for all data	0.0161/0.0405	0.0186/0.0413
Data/parameters	294/20	471/21
Goodness-of-fit on F^2	1.152	1.284
Extinction coefficient	0.00014(3)	0.00030(4)
BASF	0.256	0.068
Diff. Fourier residues/e$^-$ Å^{-3}	−2.04/+1.54	−2.25/+3.00

Table 3. Atom positions and equivalent isotropic displacement parameters (pm^2) from single-crystal X-ray diffraction studies for Hf_6Al_7 and $Hf_{4.44(1)}Nb_{1.56(1)}Al_7$ ($R\bar{3}m$, W_6Fe_7 type, $Z = 3$). U_{eq} is defined as one third of the trace of the orthogonalized U_{ij} tensor. Refined site occupancies are listed.

Atom	Wyckoff position	x	y	z	U_{eq}	occ.
Hf_6Al_7						
Hf1	6*c*	0	0	0.33437(2)	52(2)	1
Hf2	6*c*	0	0	0.14936(2)	53(2)	1
Hf3	6*c*	0	0	0.04577(2)	63(2)	1
Al1	3*b*	0	0	1/2	72(10)	1
Al2	18*h*	0.5025(3)	$-x$	0.09060(6)	69(4)	1
$Hf_{4.44(1)}Nb_{1.56(1)}Al_7$						
Hf1	6*c*	0	0	0.33453(2)	44(1)	1
Hf2	6*c*	0	0	0.14878(2)	47(1)	1
Hf/Nb3	6*c*	0	0	0.04413(2)	47(2)	0.22(1)/0.78(1)
Al1	3*b*	0	0	1/2	32(5)	1
Al2	18*h*	0.50220(14)	$-x$	0.08949(4)	40(2)	1

Table 4. Chemical compositions determined by SEM/EDX for Hf_6Al_7 and nominal $Hf_4Nb_2Al_7$.

	Theoretical composition [at%]			Experimental composition [at%]		
Compound	Hf	Nb	Al	Hf	Nb	Al
Hf_6Al_7	46.2	–	53.8	45(2)	–	55(2)
$Hf_4Nb_2Al_7$	30.8	15.4	53.8	28(2)	16(2)	56(2)

2.4. ^{27}Al Solid-State NMR

The ^{27}Al MAS-NMR spectra were recorded at 104.31 MHz on an Avance III 400 WB spectrometer (Bruker, Billerica, USA) using magic-angle spinning (MAS) conditions. The samples were ground to a fine powder and mixed with an appropriate amount of NaCl (sample:NaCl = 1:9), to reduce the density and the electrical conductivity of the sample. The diluted samples were loaded into cylindrical ZrO_2 rotors with a diameter of 4 mm and spun at the magic angle with frequencies between 8 and 13 kHz. All experiments conducted were single-pulse experiments with typical pulse length of 0.83 μs and relaxation delays of 1 s. Resonance shifts were referenced to a 1 molar aqueous $AlCl_3$ solution. The NMR spectra were recorded using the Bruker TOPSPIN software,[30] the analysis was performed with the help of the DMFIT program package.[31] The extracted data is compiled in **Table 5**.

15213749, 2025, 11, Downloaded from https://onlinelibrary.wiley.com/doi/10.1002/zaac.202500044 by Universitatsbibliothek Der, Wiley Online Library on [11/08/2025]. See the Terms and Conditions (https://onlinelibrary.wiley.com/terms-and-conditions) on Wiley Online Library for rules of use; OA articles are governed by the applicable Creative Commons License

Table 5. Summary of the NMR observables of W_6Fe_7 type Hf_6Al_7 and its ternary coloring variant $Hf_4Nb_2Al_7$. The data was extracted from the DMFit simulation of the ^{27}Al MAS-NMR spectra with δ being the resonance shift (in ppm), C_Q the quadrupolar parameter (in kHz), η_Q the asymmetry parameter, *d*Cs chemical shift anisotropy parameter (in ppm). Theoretically calculated values from Density Functional Theory (DFT) are given with the subscript *calc*.

Compound	Site	δ	$C_{Q,calc}$	$\eta_{Q,calc}$	$C_{Q,exp}$	$\eta_{Q,exp}$	*d*Cs
Hf_6Al_7	Al1 (3*b*)	n.d.	2698	0.000	–	–	–
	Al2 (18*h*)	273	1816	0.220	3054	–	102
$Hf_4Nb_2Al_7$	Al1 (3*b*)	n.d.	1915	0.000	–	–	–
	Al2 (18*h*)	184	1483	0.738	–	–	–

2.5. Physical Property Measurements

The polycrystalline samples of Hf_6Al_7 and nominal $Hf_4Nb_2Al_7$ were investigated by temperature dependent magnetic susceptibility measurements at external fields up to 80 kOe (1 kOe = 7.96×10^4 A m^{-1}). The samples were glued to silica paddles using a low temperature varnish (General Electrics) and attached to the sample holder rod of a Vibrating Sample Magnetometer option of a Physical Property Measurement System (PPMS) by Quantum Design (San Diego, USA). The magnetization data *M*(*T*) of the samples was investigated in the temperature range between 2.5 and 300 K with an applied field of 10 kOe.

Table 6. Calculated total energies of Hf_6Al_7 and the three potential coloring variants for $Hf_4Nb_2Al_7$.

Compound	Nb occupied site	Total energy [eV]
Hf_6Al_7	–	−342.530
$Hf_4Nb_2Al_7$	Hf1 (6*c*)	−325.188
$Hf_4Nb_2Al_7$	Hf2 (6*c*)	−325.196
$Hf_4Nb_2Al_7$	Hf3 (6*c*)	−328.438

2.6. Quantum-Chemical Calculations

Electronic structure calculations were performed on Hf_6Al_7 and $Hf_4Nb_2Al_7$, the latter in a fully ordered variant using the projector augmented wave method of Blöchl[32,33] coded in the Vienna ab initio simulation package (VASP).[34,35] VASP calculations employed the potentials Hf_sv, Nb_sv, and Al. The cutoff energy for the plane wave calculations was set to 800 eV, and the Brillouin zone integration was carried out using a *k*-point mesh with a spacing of ≈0.02 ($11 \times 11 \times 3$) using the Monkhorst Pack algorithm.[36] The exchange–correlation effects were accounted for within the generalized gradient approximation GGA according to Perdew, Burke, and Ernzerhof.[37] The calculations were conducted starting from the experimental crystal data

Table 7. Löwdin charges and bonding interactions alongside their ICOBI values for Hf_6Al_7 and $Hf_4Nb_2Al_7$.

atom1	Löwdin Charge	atom2	#	*d* (pm)	ICOBI	atom1	Löwdin Charge	atom2	#	*d* (pm)	ICOBI
Hf_6Al_7						**$Hf_4Nb_2Al_7$**					
Hf1 (6*c*)	+0.51	Al2	3	299.1	0.24	Hf1 (6*c*)	+0.44	Al2	3	294.3	0.23
		Al2	3	303.6	0.22			Al2	3	298.7	0.21
		Hf1	3	304.9	0.34			Hf1	3	301.5	0.31
		Hf3	3	330.8	0.25			Nb	3	326.8	0.25
		Hf3	3	332.9	0.25			Nb	3	328.8	0.24
Hf2 (6*c*)	+0.65	Hf3	1	300.6	0.40	Hf2 (6*c*)	+0.51	Nb	1	295.2	0.40
		Al1	3	309.0	0.22			Al1	3	305.5	0.21
		Al2	3	312.1	0.19			Al2	3	307.0	0.19
		Al2	6	314.9	0.19			Al2	6	310.8	0.18
		Hf2	3	321.1	0.26			Hf2	3	317.3	0.29
Hf3 (6*c*)	+0.35	Hf3	1	262.1	0.70	Nb (6*c*)	+1.16	Nb	1	257.4	0.90
		Al2	6	293.8	0.23			Al2	6	290.2	0.22
		Hf2	1	300.6	0.40			Hf2	1	295.2	0.40
		Hf1	3	330.8	0.25			Hf1	3	326.8	0.25
		Hf1	3	332.9	0.25			Hf1	3	328.8	0.24
Al1 (3*b*)	−0.35	Al2	6	269.2	0.33	Al1 (3*b*)	−0.48	Al2	6	265.1	0.30
		Hf2	6	309.0	0.22			Hf2	6	305.5	0.21
Al2 (18*h*)	−0.44	Al2	2	264.0	0.35	Al2 (18*h*)	−0.62	Al2	2	261.1	0.30
		Al2	2	264.0	0.40			Al2	2	261.1	0.33
		Al1	1	269.2	0.33			Al1	1	265.1	0.30
		Hf3	2	293.8	0.23			Nb	2	290.2	0.22
		Hf1	1	299.1	0.24			Hf1	1	294.3	0.23
		Hf1	1	303.6	0.22			Hf1	1	298.7	0.21
		Hf2	1	312.1	0.19			Hf2	1	307.0	0.19
		Hf2	2	314.9	0.19			Hf2	2	310.8	0.18

15213749, 2025, 11, Downloaded from https://onlinelibrary.wiley.com/doi/10.1002/zaac.202500044 by Universitatsbibliothek Der, Wiley Online Library on [11/08/2025]. See the Terms and Conditions (https://onlinelibrary.wiley.com/terms-and-conditions) on Wiley Online Library for rules of use; OA articles are governed by the applicable Creative Commons License

and the whole cell underwent constrained geometry relaxation where the positional parameters had to be fixed. For $Hf_4Nb_2Al_7$, three models were employed with Nb fully replacing either Hf1, Hf2, or Hf3. The results are shown in **Table 6**.

For the optimized structures, the electronic structures of Hf_6Al_7 and $Hf_4Nb_2Al_7$ were projected from the plane-wave base onto a local orbital basis set using the LOBSTER (Local Orbital Basis Suite Towards Electronic-Structure Reconstruction) program package.[38–42] Based on these projections, the local density-of-states-matrices can be accessed enabling the calculation of Löwdin-related gross populations as well as atomic charges.[43] In addition, the recently introduced crystal orbital bond index (COBI) can be derived.[44] The COBI can be rationalized as the solid state pendant to the molecular bond index as introduced by Wiberg and Mayer.[45,46] When integrating the COBI values (then called ICOBI), they correspond to the covalent bond orders within the context of solid-state materials. The results of the chemical bonding analysis are given in **Table 7**.

3. Results

3.1. Synthesis and Powder X-Ray Diffraction

A sample with the element ratios Hf:Nb:Al of 4:1:7 was prepared, in analogy to Hf_4VAl_7, which is a new ternary ordering variant of the hexagonal Laves phase $MgZn_2$,[12] as reported recently.[8] The powder X-ray diffraction pattern (**Figure 1**a) indicates the formation of a multiphase mixture. Besides the hexagonal $MgZn_2$ type $Hf(Nb_{1-x}Al_x)_2$ also a rhombohedral phase could be identified. According to Pearson's Crystal Data,[1] only one compound has been reported in the ternary system Hf–Nb–Al, which is $Hf_{3.6}Nb_{2.3}Al_{7.1}$.[14] $Hf_{3.6}Nb_{2.3}Al_{7.1}$ crystallizes in the rhombohedral crystal system with space group $R\bar{3}m$ in the W_6Fe_7 type structure.[6] The sole report on this phase states that Hf, Nb, and Al show mixing on all three crystallographically independent Hf positions with the relative ratios of 0.6 Hf, 0.383 Nb, and 0.017 Al. A mixing of Hf and Nb indeed seems likely, since both elements tend to occupy cavities in a polyanionic framework, examples are $Nb(Cu_{0.5}Al_{0.5})_2$ or $Nb_6Ni_{3.1}Al_{3.9}$.[1] However, aluminum usually plays its role as a network-forming element, therefore mixing of Al onto the three Hf positions seems odd, especially with respect to the coordination environments of the Hf positions (Frank–Kasper polyhedra with CN = 14–16).

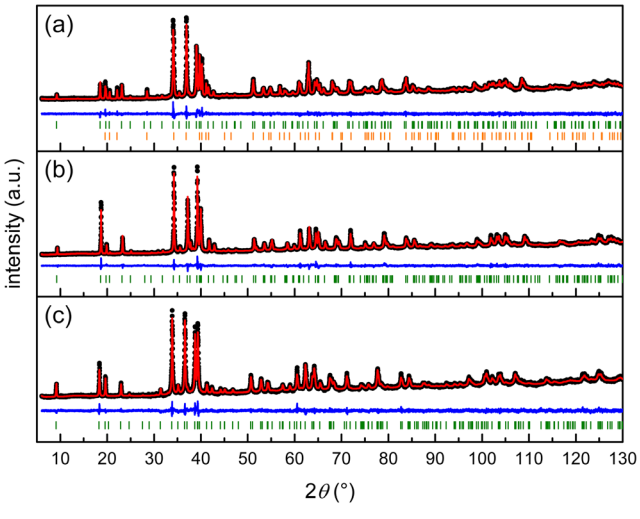

Figure 1. Rietveld refinements of different powder X-ray diffraction patterns. a) nominal Hf_4NbAl_7, b) on stoichiometry $Hf_4Nb_2Al_7$, and c) binary Hf_6Al_7. Collected data are shown as black dots, the refinement as red, and the difference as blue line. Green ticks indicate the Bragg positions of the rhombohedral W_6Fe_7 type compounds and orange ticks the $MgZn_2$ type structure.

A refinement of the site occupation factors in our sample clearly suggested that only the Hf3 position is substituted by Nb. Therefore, we decided to target the composition $Hf_4Nb_2Al_7$, where one of the three 6*c* sites (all Hf) could be solely occupied by Nb if a fully ordered structure forms. Regarding the respective coordination environments, the Hf3 position, as already observed, was expected to be the most suited one for hosting the Nb atoms due to the smallest CN (CN = 14). Syntheses with this on-stoichiometry composition led to X-ray pure compounds already in the first try (Table S1 (Supporting Information), #1). To enhance ordering of Nb and Hf atoms, the sample was annealed at 1123 K for 192 h. Based on the obtained powder X-ray diffraction data from the annealed sample (Figure 1b), the question whether the reported mixing of Hf, Nb, and Al on the three ($3 \times 6c$) crystallographic sites is real was addressed. While the positions Hf1, Hf2, Al1, and Al2 were fully occupied with the respective elements, the third 6*c* position was found to be mixed-occupied by ≈86% Nb alongside ≈14% Hf (Table 2 and 3). Due to this off-stoichiometry observed both in the powder and in the single crystal (vide infra), several syntheses with varying compositions according to $Hf_{4-x}Nb_{2+x}Al_7$ with $x = 0.22$ to 1 and different annealing strategies were conducted (Table S1 (Supporting Information), #2–8). Interestingly, all of them resulted in a similar Nb/Hf mixing on the Hf3 position leading to the assumption that the Hf3 site can only be occupied with ≈85–87% Nb despite the fact that no side phases were observed until a composition of $Hf_3Nb_3Al_7$. However, during analysis of the powder X-ray diffraction patterns, it became apparent that the respective main phase showed different lattice parameters. This observation was not further investigated.

Since the ternary compound with the nominal composition $Hf_4Nb_2Al_7$ readily formed, the binary phase Hf_6Al_7 was targeted. Here, it was observed that the compound could only be obtained by arc-melting the elements (Figure 1c, Table S1 (Supporting Information), #9&10). During subsequent syntheses, it was investigated if the sample mass plays a role, since the sample mass used in during arc-melting influences the cooling rate of the sample sometimes leading to the formation of *meta*-stable high-temperature phases. However, no dominant effect was observed. Thermal treatment of samples containing side phases after arc-melting did not yield pure samples based on X-ray diffraction (Table S1 (Supporting Information) #11). Different annealing strategies of the arc-melted beads right after synthesis (without analysis) in parts led to the formation of the targeted Hf_6Al_7; however, again, no single-phase samples according to

15213749, 2025, 11, Downloaded from https://onlinelibrary.wiley.com/doi/10.1002/zaac.202500044 by Universitatsbibliothek Der, Wiley Online Library on [11/08/2025]. See the Terms and Conditions (https://onlinelibrary.wiley.com/terms-and-conditions) on Wiley Online Library for rules of use; OA articles are governed by the applicable Creative Commons License

powder X-ray diffraction were obtained (Table S1 (Supporting Information) #12–16).

3.2. Single-Crystal X-Ray Diffraction and Structure Refinement

From the single-phase samples of Hf_6Al_7 and nominal $Hf_4Nb_2Al_7$, single crystals were isolated and prepared for the diffraction experiments as stated before. The automated indexing routine identified the correct unit cell right away; however, all investigated crystals had additional domains stuck to them (**Figure 2**, red circles). The reflections of these non-merohedral twin domains do not overlap with those of the main domain and can be separated. Structure solutions and refinements were based on the data obtained from the powder X-ray diffraction experiments with Nb partially occupying one of the 6*c* positions (Hf3 site). The refinement of both data sets led to relatively high *R*-values (e.g., ≈14% wR_2 and ≈6% R_1 for $Hf_4Nb_2Al_7$) alongside high residual electron densities (13 e^- for Hf_6Al_7; 24–57 e^- for $Hf_4Nb_2Al_7$). The reconstructed reciprocal layers (Figure 2a,c) clearly indicate the presence of obverse/reverse twinning, with a twofold rotational axis along [001] being the twinning element. After introducing the twin law (–1 0 0, 0 –1 0, 0 0 1), the residual electron densities and the *R*-values dropped to the values given in Table 2. Details on the potential twin laws are given in Figure S4 of the electronic Supporting Information.

For Hf_6Al_7, no mixing between Hf and Al was observed; however, for nominal $Hf_4Nb_2Al_7$, mixing of Hf and Nb was observed on the Hf3 site. In agreement with the powder X-ray data, the former Hf3 position is occupied by 78(1)% Nb and 22(1)% Hf leading to a refined overall composition of $Hf_{4.44(1)}Nb_{1.56(1)}Al_7$. No further mixed occupied sites were observed. After the introductions of the twin law and the mixed occupied atomic position, the difference Fourier analysis showed no significant electron density minima or maxima.

Details of the structure determination, atomic parameters and interatomic distances can be found in Table 3–5. CSDs 2420799 and 2420800 contain the supplementary crystallographic data for this paper. These data can be obtained free of charge from The Cambridge Crystallographic Data Centre via www.ccdc.cam.ac.uk/data_request/cif.

3.3. Crystal Chemistry

The crystal structure of Hf_6Al_7 can be described in two ways. One can focus on the Al substructure in view of a polyanion as it is often done for ternary intermetallic compounds. In Hf_6Al_7, the Al1 atoms are surrounded by the Al2 atoms in a distorted trigonal anti-prismatic coordination environment forming three layers, which are stacked along [001] in an ⋯*ABC*⋯ sequence. The Hf2 atoms reside in cavities formed by the Al substructure. The Hf1 and Hf3 atoms connect two of these layers (**Figure 3**a). As a side note, the Hf2-Al layers are a cutout of the hexagonal $MgZn_2$ type structure.[12,19]

An alternative is the description via the respective coordination polyhedra (Figure 3b) since the compound represents a Frank–Kasper phase. All five crystallographic positions exhibit spherical coordination environments with CNs between 12 and 16. The coordination polyhedra are shown in **Figure 4**. The polyhedra of Hf1, Hf2, and Al2 are connected along the *c*-axis via common Al_3 triangles. The Hf3 atoms finally are a corner of the Hf2 coordination environment, therefore, the Hf2 and Hf3 polyhedra interpenetrate. When looking at the interatomic distances, one realizes that the Hf–Hf interactions are between 302 and 335 pm, except for one shorter Hf3–Hf3 distance with 267 pm (single crystal data). While the long distances are above the sum of the covalent radii (r_{cov}(Hf) = 144 pm),[47] this short interaction points towards somehow strong covalent bonding interactions (vide infra). Such short Hf–Hf interactions are rather rare; structurally fully ordered examples are HfIr (262 pm)[48] or $HfTe_2$ (266 pm).[49] In comparison with elemental Hf (d(Hf–Hf) = 332 and 334 pm),[50] the distances are shorter indicating somehow covalent bonding interactions. The Hf–Al interactions range between 296 and 316 pm, which is significantly longer than the sum of the covalent radii (144 + 125 = 269 pm)[47] but in line with other binaries such as $HfAl_2$ ($MgZn_2$ type, 311–312 pm)[9] or HfAl (TlI type, 279–308 pm).[51] The Al–Al interactions, finally, range between 261 and 271 pm, which is also in the typical range

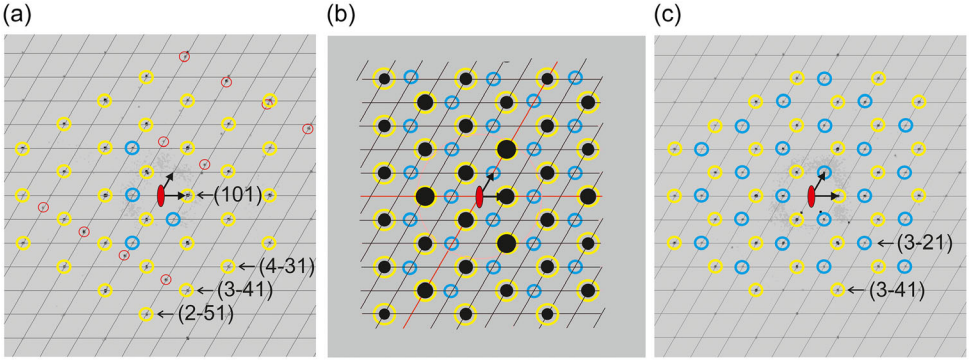

Figure 2. Reconstructed reciprocal *hk*1 layers of a) Hf_6Al_7, b) theoretical diffraction pattern created with XPrep,[68] and c) $Hf_4Nb_2Al_7$. Yellow circles indicate the reflections of the main domain (*obverse*), blue circles indicate the reflections of the twin domain (*reverse*), and red circles indicate the nonmerohedral twin domain. Selected reflections are indexed. The reflection condition for space group $R\bar{3}m$ is: $-h + k + l = 3n$ with $l = 1$.

Journal of Inorganic and General Chemistry
ZAAC
Zeitschrift für anorganische und allgemeine Chemie

15213749, 2025, 11, Downloaded from https://onlinelibrary.wiley.com/doi/10.1002/zaac.202500044 by Universitatsbibliothek Der, Wiley Online Library on [11/08/2025]. See the Terms and Conditions (https://onlinelibrary.wiley.com/terms-and-conditions) on Wiley Online Library for rules of use; OA articles are governed by the applicable Creative Commons License

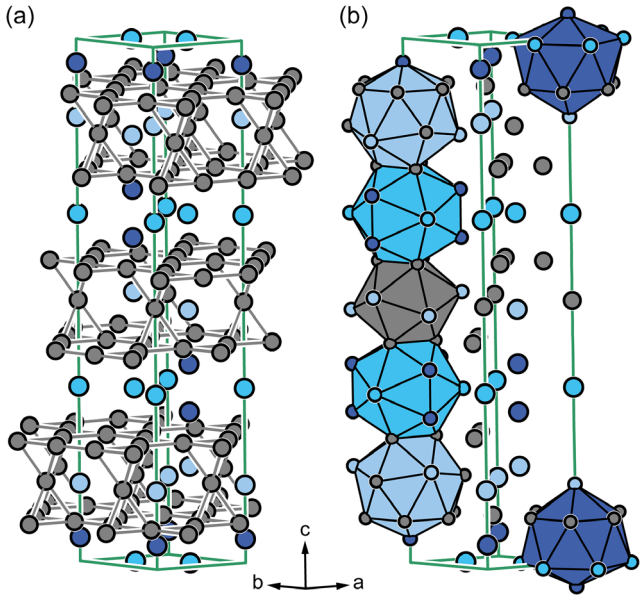

Figure 3. Crystal structure of Hf_6Al_7. a) Representation highlighting the polyanion formed by the Al atoms. b) Polyhedra representation. Al atoms are shown as grey spheres, Hf1 as light blue, Hf2 as cyan, and Hf3 as dark blue spheres.

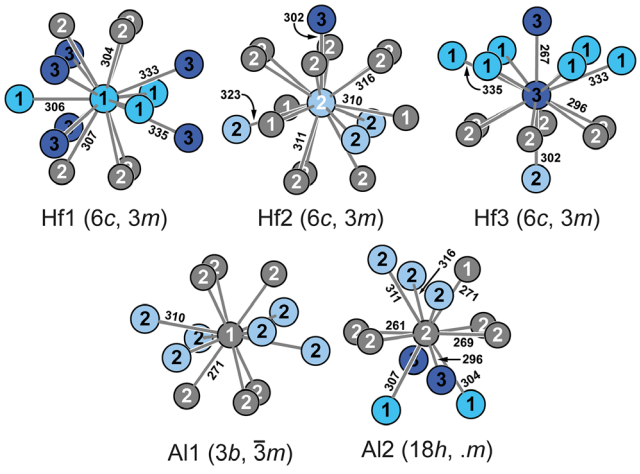

Figure 4. Coordination environments of the different crystallographically independent atomic positions in binary Hf_6Al_7. Al atoms are shown as grey spheres, Hf1 as light blue, Hf2 as cyan, and Hf3 as dark blue spheres. Interatomic distances are given in pm.

of intermetallic Al compounds (269 pm in HfAl[51] and 260–269 pm in $HfAl_2$[9]).

Upon substitution of Hf by Nb in nominal $Hf_4Nb_2Al_7$, the crystal chemistry remains the same rendering $Hf_4Nb_2Al_7$ a coloring variant of Hf_6Al_7.[52] In the following paragraph, the fully ordered denomination will be used for a better readability, knowing that the Hf/Nb3 position contains the above-mentioned occupational mixing. The Hf–Hf and Hf–Nb distances now are 300–330 pm long while the Nb–Nb interactions is now shorter with 253 pm. Similar distances can be found in the W_5Si_3 type structures (*I*4/*mcm*) given in the Pearson database.[1] From a molecular point of view, different complexes with a wide range of Nb–Nb interactions were reported. These range from nonbonding via intermediate distances between 260 and 280 pm for example in binuclear alkoxide complexes (d(Nb–Nb) = 261 pm),[53] down to extremely short Nb—Nb bonds reported by Cotton and coworkers as well as Gambarotta et al. with only 220 pm[54] and 226 pm, respectively.[55] The Hf/Nb–Al interactions now range between 293 and 313 pm. The Al–Al distances now are between 259 and 270 pm. Overall, all distance are shorter than before, in line with the smaller covalent radius of Nb (134 pm) versus Hf (144 pm).[47]

The question that arises is why is only the Hf3 position substituted by Nb and none of the other two. One reason might be the difference of the CNs of Hf1-Hf3, which can also be caused by the smaller covalent radius. Another possibility could be the shortening of the Nb–Nb distance leading to the formation of a more bonding interaction (vide infra).

3.4. ^{27}Al NMR Investigations

Since solid-state NMR spectroscopy is a local probe,[56] in principle, one would expect one resonance per crystallographically independent Al site. Therefore, this technique can be used to verify crystal structures. This has shown before in the cases of $Ba_3Al_4Pt_4$ (own type),[57] $ZrAl_2$[11] and $HfAl_2$,[8] or the $AEAl_4$ series (AE = Ca–Ba)[58] where all of these compounds have two different Al positions. In $Sr_2Al_8Pt_3$, the three Al sites could be resolved[59] and in YAl_5Pt_3; finally, all five resonances could be observed.[60]

Hf_6Al_7 and nominal $Hf_4Nb_2Al_7$ contain two different crystallographic Al sites; therefore, in their ^{27}Al MAS-NMR spectra also, two resonances are expected. Full spectra as well as the zoomed region of the central transitions are depicted in **Figure 5**a,b. The spectrum of Hf_6Al_7 shows one relatively sharp central transition originating from the $|+1/2\rangle \leftrightarrow |-1/2\rangle$ transition. The presence of quadrupolar interactions due to ^{27}Al being a $I = 5/2$ nucleus causes the observed spinning side band manifold based on the satellite transitions $|\pm1/2\rangle \leftrightarrow |\pm3/2\rangle$ and $|\pm3/2\rangle \leftrightarrow |\pm5/2\rangle$. However, the expected second signal is not clearly visible. This can have three reasons: 1) the site multiplicities are 18*h* and 3*b*, resulting in an expected signal ratio of 6:1, 2) a significant overlap of both signals, and 3) different quadrupolar coupling constants (C_Q) for the two Al sites, leading to a different degree of broadening of the resonances. The latter has been observed in the $MgZn_2$ type compounds $ZrAl_2$ and $HfAl_2$.[8,11] The quadrupolar coupling constants extracted from the DFT calculations (Table 5), however, are not that significantly different, excluding the reason number three. At a closer look (Figure 5b), a slight asymmetry of the signal of Hf_6Al_7 (black line) marked with the black arrow can be observed, leading to the assumption that an overlap of the signals seems the likeliest explanation. Taking the DFT-based asymmetry (η_Q) and quadrupolar coupling constants (C_Q) as starting values for the simulation, a significantly larger quadrupolar coupling constant can be deduced from the fit of the intensity profile of the spinning side bands (Table 5, Figure S5, Supporting Information).

When switching to the spectrum of nominal $Hf_4Nb_2Al_7$, two aspects are visible right away. Firstly, the signal is broadened

15213749, 2025, 11, Downloaded from https://onlinelibrary.wiley.com/doi/10.1002/zaac.202500044 by Universitatsbibliothek Der, Wiley Online Library on [11/08/2025]. See the Terms and Conditions (https://onlinelibrary.wiley.com/terms-and-conditions) on Wiley Online Library for rules of use; OA articles are governed by the applicable Creative Commons License

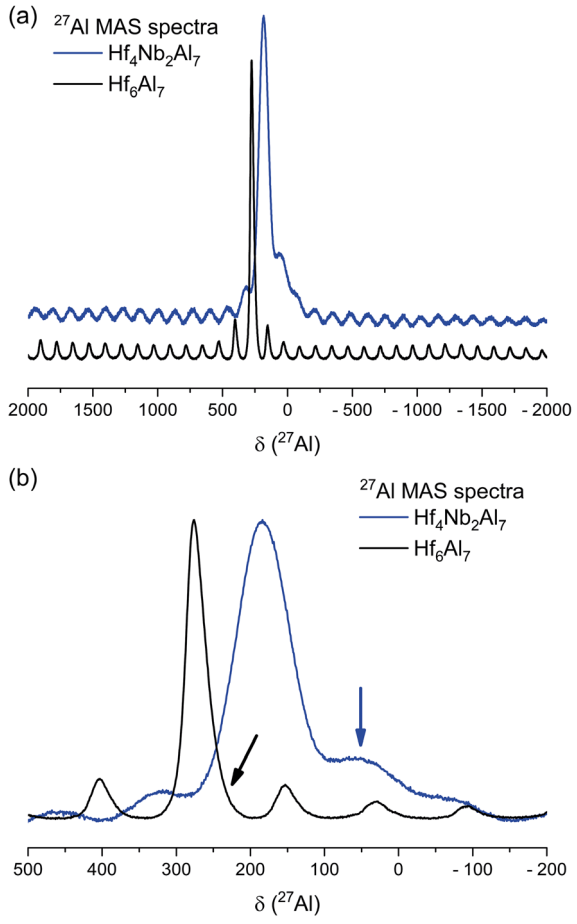

Figure 5. ^{27}Al MAS-NMR spectra of Hf_6Al_7 (black line) and nominal $Hf_4Nb_2Al_7$ (blue line). a) Full spectra of both compounds, the spectrum of nominal $Hf_4Nb_2Al_7$ is shifted along *y* for a better visibility. b) Zoomed spectra of Hf_6Al_7 (black line) and nominal $Hf_4Nb_2Al_7$. The arrows indicate the possible positions of the second signal.

compared to the one of Hf_6Al_7 and secondly, a bump at a higher resonance frequency (lower resonance shift) is visible. Both is directly linked to the incorporation of Nb into the structure. As described above, a random mixing of Nb and Hf is observed, leading to the refined formula of $Hf_{4.44(1)}Nb_{1.56(1)}Al_7$ (single crystal data), being responsible for the line broadening. However, this effect is not as pronounced as for other examples of solid solutions (e.g., $Zr(V_{1-x}Al_x)_2$,[11] $Na_2Au_{3-x}Al_{1+x}$[61] or Sc*T*Al,[62] and $Sc(T_{0.5}T'_{0.5})_2Al$[63]). Due to the different electronic situation of Nb in comparison with Hf, a shift of about 100 ppm of the main resonance is observed; in addition, a more pronounced second resonance, marked by the blue arrow in Figure 5b, is visible most likely originating from the second Al position.

3.5. Physical Properties

Rhombohedral Hf_6Al_7 as well as its nominal substitutional coloring variant $Hf_4Nb_2Al_7$ was investigated via temperature-depending susceptibility measurements between 2.5 and 300 K at an applied external field of 10 kOe. Due to the absence of localized unpaired electrons but metallic character of the compounds, both samples show Pauli-paramagnetism over the whole investigated temperature range. **Figure 6** depicts the magnetic susceptibility data for the two investigated compounds. It is clearly visible that both traces show an overall temperature independent behavior with an upturn at low temperatures originating from traces of Curie-paramagnetic impurities.

3.6. Quantum–Chemical Calculations

Quantum–chemical calculations were performed on the DFT level using the experimental lattice parameters and atomic positions as starting points. The idealized structures, with respect to mixed occupancies, were used. In all cases, the atomic positions had to be fixed in order to get converged results. To understand the selective mixing of Hf and Nb on the Hf3 position in $Hf_4Nb_2Al_7$, three ordered models were calculated with Nb occupying either the Hf1, Hf2, or Hf3 position of the binary variant in a fully ordered fashion. Total energy calculations clearly showed (Table 6) that the observed ordering variant with Nb on the Hf3 position is energetically more stable (−328.438 eV) compared to the other two (Nb on Hf1: −325.188 eV; Nb on Hf2: −325.196 eV) underlining the experimental results.

Subsequently, the chemical bonding of Hf_6Al_7 and $Hf_4Nb_2Al_7$ was addressed using Löwdin charges and ICOBI (integrated crystal orbital bond indices) values recently introduced into LOBSTER.[39,40,43,44,64] For strong covalent bonds, ICOBI values up to one can be observed; while contrasting, values near zero will indicate no (for large distances) or rather ionic interactions (for appropriate distances).[44,65] For metallic materials exhibiting delocalization of their bonding,[66] multicenter bonding is observed. This is rationalized by ICOBI values somewhere between 0 and 1. Recent reports have shown the application towards intermetallic compounds.[64,67] Table 7 lists the Löwdin charges alongside the ICOBI values for selected interactions. For both binary Hf_6Al_7 and ternary $Hf_4Nb_2Al_7$, the Al atoms carry negative Löwdin charges, rendering these compounds aluminides, as expected from the electronegativities, while the Hf

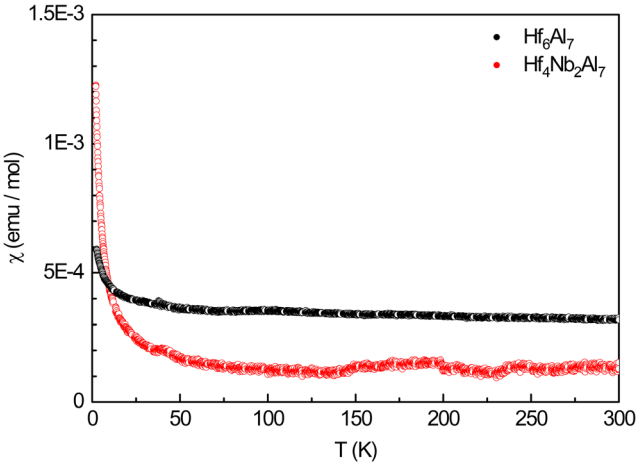

Figure 6. Magnetic susceptibility data of Hf_6Al_7 and nominal $Hf_4Nb_2Al_7$. Measurements were conducted in zero-field cooled mode at an applied field of 10 kOe.

and Nb atoms are cationic. One interesting aspect concerns the charges of the Hf3/Nb atoms. While Hf3 carries the lowest positive charge of +0.35, Nb has a charge of +1.16. In turn, the Löwdin charges of the Al atoms in $Hf_4Nb_2Al_7$ increase, but at the same time, the charges of Hf1 and Hf2 decrease for compensation.

When looking at the ICOBI values, the Al–Al interactions are in the typical range of other intermetallic compounds.[64,67] The Hf–Al interactions, however, are significantly stronger (ICOBI 0.19–0.23) when compared to, e.g., the Sr–Al interactions in $SrAl_8Rh_2$ (ICOBI 0.02–0.04). One striking feature of both Hf_6Al_7 and $Hf_4Nb_2Al_7$ are the short Hf3–Hf3 (DFT: 262.1 pm)/Nb–Nb (DFT: 257.4 pm) interaction. For the binary compound, the ICOBI value is 0.70, indicating a strong covalent contribution (70% of a single bond); for the ternary phase, this value increases even further to 0.90, in line with a covalent single Nb—Nb bond.

4. Conclusion

Motivated by our recent discovery of Hf_4VAl_7, we tried to extend the knowledge on this singular compound by replacing vanadium with other early transition metals. With Hf_6Al_7, a new binary compound crystallizing in the W_6Fe_7 type structure (μ phase, Frank–Kasper phase) as well as its ternary coloring variant, nominal $Hf_4Nb_2Al_7$, was discovered starting from the results of a synthesis targeting nominal "Hf_4NbAl_7." The compounds were synthesized from the elements and structurally characterized. While the Nb-containing phase forms quite readily, getting phase pure samples of binary Hf_6Al_7 was challenging. The Nb substitution was found to occur only on one of the three crystallographic Hf positions of the prototype with the smallest coordination polyhedron. Quantum-chemical calculations indicate that the substitution on the Hf3 site is, compared to the other possibilities, energetically favored in line with the smaller covalent radius of Nb versus Hf alongside the formation a Nb—Nb single bond. Both compounds are Pauli-paramagnets as expected based on their metallic nature and the absence of localized unpaired electrons. ^{27}Al solid-state NMR investigations revealed only one signal, contradicting the expected two signals based on the crystal structure. However, the relative ratio of the two signals is expected to be 6:1 leading to one strong signal alongside a second one being potentially overlapped with the main signal or rotational sidebands.

It is interesting to note that Hf_6Al_7, besides $HfAl_2$ and Hf_4Al_3, is already the third Frank–Kasper phase in the binary system Hf–Al. In contrast to Hf_4VAl_7 (ordering variant of $MgZn_2$), however, $Hf_4Nb_2Al_7$ exhibits a mixing on the Hf positions rather than the Al positions. This raises several questions: 1) can a trend of the substitutional behavior of the third element in binary Hf–Al Frank–Kasper phases be established? 2) Are there other ternary representatives in analogy to $Hf_4Nb_2Al_7$? 3) Are there further substitutional variants of the $MgZn_2$ type $HfAl_2$ or the W_6Fe_7 type Hf_6Al_7? 4) Are ternary (ordered) substitutions possible in Hf_4Al_3? And finally 5) can other *M*—*M* single bonds be established in the W_6Fe_7 type structure?

Acknowledgements

Instrumentation and technical assistance for the X-ray diffraction part this work were provided by the Service Center X-ray Diffraction, with financial support from Saarland University and German Research Foundation (project numbers INST 256/349-1 and INST 256/582-1). Instrumentation and technical assistance for the NMR part were provided by the Core Facility NMR with financial support from Saarland University and German Research Foundation DFG (INST 256/384-1). This research was funded by Universität Münster and German Research foundation (INST 211/1034-1).

Open Access funding enabled and organized by Projekt DEAL.

Conflict of Interest

The authors declare no conflict of interest.

Author Contributions

All authors have accepted responsibility for the entire content of this submitted manuscript and approved the submission.

Data Availability Statement

The data that support the findings of this study are available from the corresponding author upon reasonable request.

Keywords: density functional theory calculations · intermetallics · single-crystal · solid-state NMR

[1] P. Villars, K. Cenzual, *Pearson's Crystal Data: Crystal Structure Database for Inorganic Compounds*, ASM International, Materials Park, Ohio, USA **2023**.
[2] A. W. Hull, *Phys. Rev.* **1917**, *10*, 661.
[3] P. Debye, *Phys. Z.* **1917**, *18*, 483.
[4] C. H. Johansson, J. O. Linde, *Ann. Phys.* **1925**, *78*, 439.
[5] G. Brauer, *Naturwissenschaften* **1938**, *26*, 710.
[6] H. Arnfelt, A. Westgren, *Jernkontorets Ann.* **1935**, *119*, 185.
[7] G. L. Chen, J. G. Wang, X. D. Ni, J. P. Lin, Y. L. Wang, *Intermetallics* **2005**, *13*, 329.
[8] E. C. J. Gießelmann, S. Engel, J. Baldauf, J. Kösters, S. F. Matar, G. Kickelbick, O. Janka, *Inorg. Chem.* **2024**, *63*, 8180.
[9] L.-E. Edshammar, S. Andersson, *Acta Chem. Scand.* **1960**, *14*, 223.
[10] L. Tarschisch, A. T. Titow, F. K. Garjanow, *Phys. Z. Sowjetunion* **1934**, *5*, 503.
[11] E. C. J. Gießelmann, L. Schumacher, S. F. Matar, S. Engel, G. Kickelbick, O. Janka, *Chem. Eur. J.* **2025**, *31*, e202404248.
[12] E. C. J. Gießelmann, R. Pöttgen, O. Janka, *Z. Anorg. Allg. Chem.* **2023**, *649*, e202300109.
[13] O. Janka, R. Pöttgen, *Z. Naturforsch.* **2024**, *79b*, 63.
[14] M. A. Fedorova, V. V. Byrnashova, E. M. Sokolovskaya, P. I. Krypyakevych, *Tezizy Dokl. Vses. Konf. Kristallokhim. Intermet. Soeden.* **1974**, *2*, 18.
[15] F. C. Frank, J. S. Kasper, *Acta Crystallogr.* **1958**, *11*, 184.
[16] F. C. Frank, J. S. Kasper, *Acta Crystallogr.* **1959**, *12*, 483.

 © 2025 The Author(s). Zeitschrift für anorganische und allgemeine Chemie published by Wiley-VCH GmbH

15213749, 2025, 11, Downloaded from https://onlinelibrary.wiley.com/doi/10.1002/zaac.202500044 by Universitatsbibliothek Der, Wiley Online Library on [11/08/2025]. See the Terms and Conditions (https://onlinelibrary.wiley.com/terms-and-conditions) on Wiley Online Library for rules of use; OA articles are governed by the applicable Creative Commons License

[17] R. Pöttgen, D. Johrendt, *Intermetallics - Synthesis, Structure, Function*, De Gruyter, Berlin, Boston **2014**.
[18] R. Pöttgen, D. Johrendt, *Intermetallics - Synthesis, Structure, Function*, De Gruyter, Berlin, Boston **2019**.
[19] O. Janka, *Comprehensive Inorganic Chemistry III*, Elsevier, Amsterdam **2023**.
[20] R. Pöttgen, T. Gulden, A. Simon, *GIT Labor-Fachz.* **1999**, *43*, 133.
[21] Bruker AXS Inc., Topas, Karlsruhe (Germany) **2014**.
[22] H. M. Rietveld, *Acta Crystallogr.* **1967**, *22*, 151.
[23] H. M. Rietveld, *J. Appl. Crystallogr.* **1969**, *2*, 65.
[24] Agilent, CrysAlis PRO, Agilent Technologies Ltd., Yarnton, Oxfordshire, England **2014**.
[25] G. Sheldrick, *Acta Crystallogr.* **2015**, *A71*, 3.
[26] G. Sheldrick, *Acta Crystallogr.* **2015**, *C71*, 3.
[27] G. M. Sheldrick, *Acta Crystallogr.* **2008**, *A64*, 112.
[28] C. B. Hübschle, G. M. Sheldrick, B. Dittrich, *J. Appl. Crystallogr.* **2011**, *44*, 1281.
[29] K. Brandenburg, Crystal Impact, Diamond, Bonn (Germany) **2022**.
[30] Bruker Corp., Topspin, Karlsruhe **2008**.
[31] D. Massiot, F. Fayon, M. Capron, I. King, S. Le Calvé, B. Alonso, J.-O. Durand, B. Bujoli, Z. Gan, G. Hoatson, *Magn. Reson. Chem.* **2002**, *40*, 70.
[32] P. E. Blöchl, *Phys. Rev. B* **1994**, *50*, 17953.
[33] G. Kresse, D. Joubert, *Phys. Rev. B* **1999**, *59*, 1758.
[34] G. Kresse, J. Furthmüller, *Phys. Rev. B* **1996**, *54*, 11169.
[35] G. Kresse, J. Furthmüller, *Comput. Mater. Sci.* **1996**, *6*, 15.
[36] H. J. Monkhorst, J. D. Pack, *Phys. Rev. B* **1976**, *13*, 5188.
[37] J. P. Perdew, K. Burke, M. Ernzerhof, *Phys. Rev. Lett.* **1996**, *77*, 3865.
[38] R. Dronskowski, P. E. Blöchl, *J. Phys. Chem.* **1993**, *97*, 8617.
[39] R. Nelson, C. Ertural, J. George, V. L. Deringer, G. Hautier, R. Dronskowski, *J. Comput. Chem.* **2020**, *41*, 1931.
[40] S. Maintz, V. L. Deringer, A. L. Tchougréeff, R. Dronskowski, *J. Comput. Chem.* **2016**, *37*, 1030.
[41] S. Maintz, V. L. Deringer, A. L. Tchougréeff, R. Dronskowski, *J. Comput. Chem.* **2013**, *34*, 2557.
[42] V. L. Deringer, A. L. Tchougréeff, R. Dronskowski, *J. Phys. Chem. A* **2011**, *115*, 5461.
[43] C. Ertural, S. Steinberg, R. Dronskowski, *RSC Adv.* **2019**, *9*, 29821.
[44] P. C. Müller, C. Ertural, J. Hempelmann, R. Dronskowski, *J. Phys. Chem. C* **2021**, *125*, 7959.
[45] I. Mayer, *Chem. Phys. Lett.* **1983**, *97*, 270.
[46] K. B. Wiberg, *Tetrahedron* **1968**, *24*, 1083.
[47] J. Emsley, *The Elements*, Clarendon Press, Oxford University Press, Oxford, New York **1998**.
[48] K. Schubert, A. Raman, W. Rossteutscher, *Naturwissenschaften* **1964**, *51*, 506.
[49] S. Mangelsen, P. G. Naumov, O. I. Barkalov, S. A. Medvedev, W. Schnelle, M. Bobnar, S. Mankovsky, S. Polesya, C. Näther, H. Ebert, W. Bensch, *Phys. Rev. B* **2017**, *96*, 205148.
[50] W. Noethling, S. Tolksdorf, *Z. Kristallogr. – Cryst. Mater.* **1925**, *62*, 255.
[51] L.-E. Edshammar, *Acta Chem. Scand.* **1961**, *15*, 403.
[52] R. Pöttgen, *Z. Anorg. Allg. Chem.* **2014**, *640*, 869.
[53] F. A. Cotton, M. P. Diebold, W. J. Roth, *Inorg. Chem.* **1985**, *24*, 3509.
[54] F. A. Cotton, J. H. Matonic, C. A. Murillo, *J. Am. Chem. Soc.* **1997**, *119*, 7889.
[55] M. Tayebani, K. Feghali, S. Gambarotta, G. P. A. Yap, *Inorg. Chem.* **2001**, *40*, 1399.
[56] C. Benndorf, H. Eckert, O. Janka, *Acc. Chem. Res.* **2017**, *50*, 1459.
[57] F. Stegemann, C. Benndorf, T. Bartsch, R. S. Touzani, M. Bartsch, H. Zacharias, B. P. T. Fokwa, H. Eckert, O. Janka, *Inorg. Chem.* **2015**, *54*, 10785.
[58] S. Engel, E. C. J. Gießelmann, L. E. Schank, G. Heymann, K. Brix, R. Kautenburger, H. P. Beck, O. Janka, *Inorg. Chem.* **2023**, *62*, 4260.
[59] F. Stegemann, T. Block, S. Klenner, Y. Zhang, B. P. T. Fokwa, C. Doerenkamp, H. Eckert, O. Janka, *Eur. J. Inorg. Chem.* **2021**, 3832.
[60] S. Engel, E. C. J. Gießelmann, L. Schumacher, Y. Zhang, F. Müller, O. Janka, *Dalton Trans.* **2024**, *53*, 12176.
[61] F. Stegemann, C. Benndorf, Y. Zhang, M. Bartsch, H. Zacharias, B. P. T. Fokwa, H. Eckert, O. Janka, *Inorg. Chem.* **2017**, *56*, 1919.
[62] M. Radzieowski, C. Benndorf, S. Haverkamp, H. Eckert, O. Janka, *Z. Naturforsch.* **2016**, *71b*, 553.
[63] C. Benndorf, O. Niehaus, H. Eckert, O. Janka, *Z. Anorg. Allg. Chem.* **2015**, *641*, 168.
[64] L. S. Reitz, J. Hempelmann, P. C. Müller, R. Dronskowski, S. Steinberg, *Chem. Mater.* **2024**, *36*, 6791.
[65] J. Simons, J. Hempelmann, K. S. Fries, P. C. Müller, R. Dronskowski, S. Steinberg, *RSC Adv.* **2021**, *11*, 20679.
[66] S. Steinberg, R. Dronskowski, *Crystals* **2018**, *8*, 225.
[67] S. Engel, M. K. Reimann, E. Svanidze, M. Krnel, N. Zaremba, M. König, O. Janka, *Z. Kristallogr.* **2025**, *240*, 1.
[68] G. M. Sheldrick, B. AXS, XPREP, Madison, WI (USA) **2008**.

Manuscript received: February 28, 2025
Revised manuscript received: April 25, 2025
Version of record online: June 16, 2025

© 2025 The Author(s). Zeitschrift für anorganische und allgemeine Chemie published by Wiley-VCH GmbH

15213749, 2025, 11, Downloaded from https://onlinelibrary.wiley.com/doi/10.1002/zaac.202500044 by Universitatsbibliothek Der, Wiley Online Library on [11/08/2025]. See the Terms and Conditions (https://onlinelibrary.wiley.com/terms-and-conditions) on Wiley Online Library for rules of use; OA articles are governed by the applicable Creative Commons License